ELSEVIER
SAUNDERS

Dent Clin N Am 49 (2005) 771–793

THE DENTAL
CLINICS
OF NORTH AMERICA

Early Caries Imaging and Monitoring with Near-Infrared Light

Daniel Fried, PhD*, John D.B. Featherstone, PhD, Cynthia L. Darling, PhD, Robert S. Jones, DDS, Patara Ngaotheppitak, Christopher M. Bühler

Department of Preventive and Restorative Dental Sciences, University of California—San Francisco, 707 Parnassus Avenue, San Francisco, CA 94143, USA

Enamel is highly transparent in the near infrared (NIR); therefore, this region of the electromagnetic spectrum is ideally suited for the development of new optical diagnostic tools for the detection and imaging of early dental caries. This article discusses the NIR optical properties of sound and demineralized dental enamel and the potential use of polarization sensitive optical coherence tomography (PS-OCT) and NIR transillumination for the imaging of dental caries.

New diagnostic tools are needed for the detection and characterization of caries lesions in the early stages of development [1]. Conventional methods, that is, visual/tactile and radiographic, have numerous shortcomings and are inadequate for the detection of the early stages of the caries process [2–4]. Radiographic methods do not have sufficient sensitivity for early lesions, particularly occlusal lesions. By the time the occlusal lesions are radiolucent, they have often progressed well into the dentin at which point surgical intervention is necessary [4–6]. At that stage in the decay process, it is too late for preventive and conservative intervention, and a large portion of carious and healthy tissue will need to be removed, often compromising the mechanical integrity of the tooth. If left untreated, the decay will eventually infect the pulp, leading to loss of tooth vitality and possible extraction. The caries process is potentially preventable and curable. If carious lesions are detected in the enamel early enough, it is likely that they can be arrested or reversed by nonsurgical means through fluoride therapy,

This work was supported by National Institutes of Health /National Institute of Dental Research grant R01-DE14698.

* Corresponding author.
E-mail address: dfried@itsa.ucsf.edu (D. Fried).

doi:10.1016/j.cden.2005.05.008 ***dental.theclinics.com***

antibacterial therapy, dietary changes, or low-intensity laser irradiation [1,7]. One cannot overstate the importance of detecting the decay in the early stage of development at which point noninvasive preventive measures can be taken to halt further decay.

Accurate determination of the degree of lesion activity and severity is of paramount importance for effective employment of the treatment strategies mentioned previously. Because optical diagnostic tools exploit changes in light scattering in the lesion, they have great potential for diagnosing whether the caries lesion is active and expanding, or arrested and remineralizing. Such data are invaluable for caries management by risk assessment in the patient and for determining the appropriate form of intervention. A nondestructive quantitative method of monitoring demineralization in vivo with high sensitivity would also be invaluable for use in short-term clinical trials for various anticaries agents such as new or modified fluoride dentifrices and antimicrobials. In particular, a method that could be employed in the relevant high-risk areas of the tooth, such as pits and fissures, would be universally useful.

Optical transillumination was used extensively before the discovery of x-rays for detection of dental caries. Over the past two decades, there has been continued interest in this method, especially with the availability of high-intensity fiberoptic-based illumination systems for the detection of interproximal lesions [8–12]. During fiberoptic transillumination (FOTI), a carious lesion appears dark because of decreased transmission owing to increased scattering and absorption by the lesion. A digital fiberoptic transillumination system, the DiFoti device, which uses visible light for the detection of caries lesions, has been developed recently (Electro-optics Sciences, Irvington, New York) [13] and received US Food and Drug Administration (FDA) approval 3 years ago. Because this system operates in the visible range, the light cannot penetrate far through enamel. NIR light can penetrate much further through all of the tooth enamel, owing to the reduced scattering in normal enamel (Fig. 1)

Teeth naturally fluoresce upon irradiation with ultraviolet (UV) and visible light. Alfano and coworkers [14] and Bjelkhagen and Sundstrom [15] demonstrated that laser-induced fluorescence of endogenous fluorophores in human teeth could be used as a basis for discrimination between carious and sound tissue. Upon illumination with near-UV and visible light and imaging of the emitted fluorescence in the range of 600 to 700 nm, carious or demineralized areas appear dark. The origin of the endogenous fluorescence in teeth in this particular wavelength range has not been established. Hafstrom-Bjorkman and coworkers [16] established an experimental relationship between the loss of fluorescence intensity and the extent of enamel demineralization. This method was subsequently labeled the QLF method for quantitative laser fluorescence. An empirical relationship between overall lesion demineralization (ΔZ) versus the loss of fluorescence was established, which can be used to monitor lesion progression on smooth

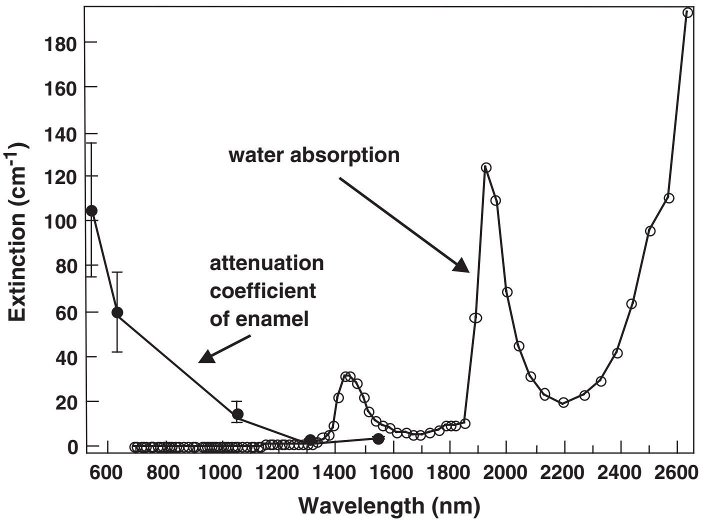

Fig. 1. Plot of the mean ± standard deviation of the attenuation coefficient for dental enamel [42,52] (filled circles) and the absorption coefficient of water [53] (open circles) versus wavelength. (*Data from* Refs. [42,52,53].)

surfaces [17–19]. Unfortunately, QLF cannot be readily applied to occlusal and interproximal lesions that constitute the majority of carious lesions. Furthermore, the fluorescence method cannot be used to provide information about the subsurface characteristics of the lesion.

Bacteria produce significant amounts of porphyrins, and dental plaque fluoresces upon excitation with red light [20]. A novel caries detection system, the Diagnodent (Kavo, Biberach/Riss, Germany), has also received FDA approval in the United States. This device uses a diode laser and a fiberoptic probe designed to detect the NIR fluorescence from porphyrins. Although this method is a major step toward better caries detection in occlusal surfaces, the principal limitation of the device is that it detects lesions in the later stage of development after which the caries has penetrated into the dentin and accumulated a considerable amount of bacterial byproducts. Moreover, the Diagnodent has a poor sensitivity (approximately 0.4) for lesions confined to enamel [21]. Fluorescence methods cannot provide depth-resolved images of demineralization or lesion severity [22,23].

OCT is a noninvasive technique for creating cross-sectional images of internal tissue structures [24]. The intensity of backscattered light is measured as a function of its axial position in the tissue. Low-coherence interferometry is used to remove selectively or gate out the component of backscattered signal that has undergone multiple scattering events, resulting in high-resolution images (<15 μm). Lateral scanning of the probe beam across the biologic tissue is then used to generate a two-dimensional intensity plot, similar to ultrasound images, called a b-scan. The one-dimensional analogue of OCT, optical coherence domain reflectometry (OCDR), was first developed as a high-resolution ranging technique for characterization of optical components [25,26]. Huang and coworkers [27] combined transverse scanning with a fiberoptic OCDR system to produce the first OCT cross-sectional images of biologic microstructure. The first images of the soft- and hard-tissue structures of the oral cavity were acquired by Colston and coworkers [28–30]. Baumgartner and coworkers [31–33] presented the first polarization-resolved images of dental caries; however, the penetration depth was limited, and the image quality was poor. Feldchtein and colleagues [34] presented high-resolution dual-wavelength 830- and 1280-nm images of dental hard tissues, enamel, and dentin caries and restorations in vivo. Wang and coworkers [35] measured the birefringence in dentin and enamel and suggested that the enamel rods acted as waveguides. The following year, Everett and colleagues [36] in conjunction with the authors presented polarization-resolved images using a high-power, 1310-nm broadband source and a bulk optic PS-OCT system. Changes in the mineral density of tooth enamel were resolvable to depths of 2 to 3 mm into the tooth. OCT has also been used to look at different restorative materials and to identify pit and fissure sealants [34,37]. Amaechi and coworkers [38,39] demonstrated that the loss of penetration depth in OCT images correlated with QLF measurements of smooth surface artificial caries. Nevertheless, most early decay is located in the highly irregular occlusal surfaces in which such methods are difficult to implement, and the authors have demonstrated that it is necessary to use PS-OCT to quantify lesion severity in topographical challenging areas such as the occlusal pits and fissures.

Optical properties of dental hard tissue in the visible and near infrared

A fundamental understanding of how NIR light propagates through sound and carious dental hard tissues is essential for the development of clinically useful optical diagnostic systems, because image contrast is based on changes in the optical properties of these tissues on demineralization. Dental hard-tissue optics is inherently complex owing to the nonhomogeneous and anisotropic nature of these biologic materials. The scattering distributions are generally anisotropic and depend on tissue orientation relative to the irradiating light source [40–43] in addition to the polarization of the incident light [44,45]. The optical properties of biologic tissue can be described completely and quantitatively by defining the optical constants, the absorption (μ_a), and scattering coefficients (μ_s), which represent the probability of the incident photons being absorbed or scattered, and the scattering phase function $\Phi(\cos(\theta))$, which is a mathematical function that describes the directional nature of scattering [46–49]. With knowledge of these parameters, light transport in dental hard tissues can be characterized completely and modeled. An accurate description of light transport in dental hard tissues relies on knowledge of the exact form of the phase function $\Phi(\cos(\theta))$ for each tissue scatterer at each wavelength [49].

Optical properties of sound enamel and dentin

Light absorption by enamel is very weak in the visible and NIR ($\mu_a < 1$ cm^{-1}, $\lambda = 400$–1300 nm) and increases in the ultraviolet ($\mu_a > 10$ cm^{-1}, $\lambda < 240$ nm) [50]. The absorption coefficient of dentin is essentially wavelength independent with a value of $\mu_a \sim 4$ cm^{-1} [51] above 400 nm. The optical behavior of enamel and dentin are dominated by scattering in the visible and NIR [50]. The scattering coefficient of enamel, μ_s, decreases with increasing wavelength from 400 cm^{-1} in the near-UV [50] to as low a value as 2 to 3 cm^{-1} at 1310 nm and 1550 nm [42,52] (see Fig. 1). At longer wavelengths, water absorption increases and dominates the attenuation [53]. The scattering of dentin is variable with position in the tooth and exceeds 100 to 200 cm^{-1} across the visible and NIR [51]. Measurement of the enamel attenuation coefficient at 1310 nm and 1550 nm was a particular challenge, because the scattering coefficient is almost two orders of magnitude lower than in the visible range, ~2 to 3 cm^{-1} at 1310 nm versus 105 cm^{-1} at 543 nm, and surface scattering can completely mask measurement of the bulk scattering properties [42].

The authors previously employed the Monte Carlo method [54,55] to determine the optical properties of dentin and enamel at 543, 632, and 1053 nm. Although the Monte Carlo method is labor and computationally intensive, it has consistently been shown to yield the most reliable values [46,49]. The accuracy of the values computed was confirmed by successfully modeling the angular-resolved scattering distributions measured for sections of various thickness from 100 μm to 2 mm in the multiple scattering regimen. The measured angular-resolved scattering distributions could not be represented by a single scattering phase function $\Phi(\cos\theta)$, and required a linear combination of a highly forward peaked phase function, a Henyey-Greenstein function, and an isotropic phase function represented by the following equation [42]:

$$\Phi(\cos\theta) = f_d + (1 - f_d)\left(\frac{(1 - g^2)}{(1 - g^2 - 2g\cos\theta)^{3/2}}\right)$$

The parameter for fraction diffuse (f_d) is defined as the fraction of isotropic scatterers. The average value of the cosine of the scattering angle (θ) is called the scattering anisotropy (g), where $g = 0.96$ and 0.93 for enamel and dentin, respectively, at 1053 nm [42]. The fraction of isotropic scatterers (f_d) was measured to be 36% for enamel and less than 2% for dentin at 1053 nm. Zijp and coworkers [40,43] reported values of $g = 0.4$ for dentin and $g = 0.68$ for enamel, calculated by taking the ratio of the forward and backward scattered light. That approach is prone to error owing to the contribution of surface scattering [42]. Most scattering biologic tissues that can be represented by a Henyey-Greenstein function have measured g values greater than 0.8 [46]. Moreover, the g value should be determined within the context of an appropriate phase function based on the nature of the scatterers in the tissue [56], and subsequently validated through a comparison of simulated scattering distributions with measured distributions of various thickness as the authors accomplished previously [42].

Optical property changes of demineralized enamel

Increased backscattering from the demineralized region of early caries lesions is the basis for the visual appearance of white spot lesions [57,58]. An increase in porosity of the lesion leads to increased scattering at the lesion surface and higher scattering in the body of the lesion, producing an increase in the magnitude of the diffuse reflectance [59]. Attempts at measuring the optical properties of dental caries have been limited to measurements of backscattered light from optically thick, multilayered sections of simulated caries lesions [59–61]. The microstructure of enamel and dentin caries lesions is complex, consisting of various turbid and transparent zones [45,62]. Highly porous demineralized areas of coronal caries appear whiter and are more opaque. During remineralization, pores and tubules are filled with mineral, and those areas are typically more transparent. There have been some attempts to measure and simulate light scattering in artificial and natural lesions [57,61,63]; however, to the authors' knowledge, there has not been a major effort to measure and quantify the optical properties of carious lesions in terms of changes in the fundamental optical constants, μ_s and μ_a, and the scattering phase function. A partial reason is the difficulty in acquiring large uniform areas for measurement by conventional means. The authors have used lasers, precision positioning stages, and a zoom video microscope system to position the laser beam accurately with a spot size of 50 to 100 μm on areas of carious lesions for direct comparison with matching high-resolution digital microradiography images (Fig. 2). A procedural difference when measuring areas of carious lesion versus sound tissue is the method of index matching. Lesion areas are highly porous, allowing index-matching fluids to imbibe into the lesion, effectively eliminating the lesion from an optical standpoint because the lesion becomes more transparent than the sound tissue.

The authors' method is predicated on the principle that carious lesions will be filled with fluid in their natural state, and that measurement in water replicates the conditions that will be encountered clinically. An NIR image of the optical attenuation through the tooth section can be acquired using a large fiber collimator (20-mm beam diameter) and an InGaAs focal plane array (FPA) that can be overlaid with the mineral density distribution taken using digital microradiography. Fig. 2 shows such an NIR image of a 200-μm thick tooth section taken with the InGaAs FPA. The white areas

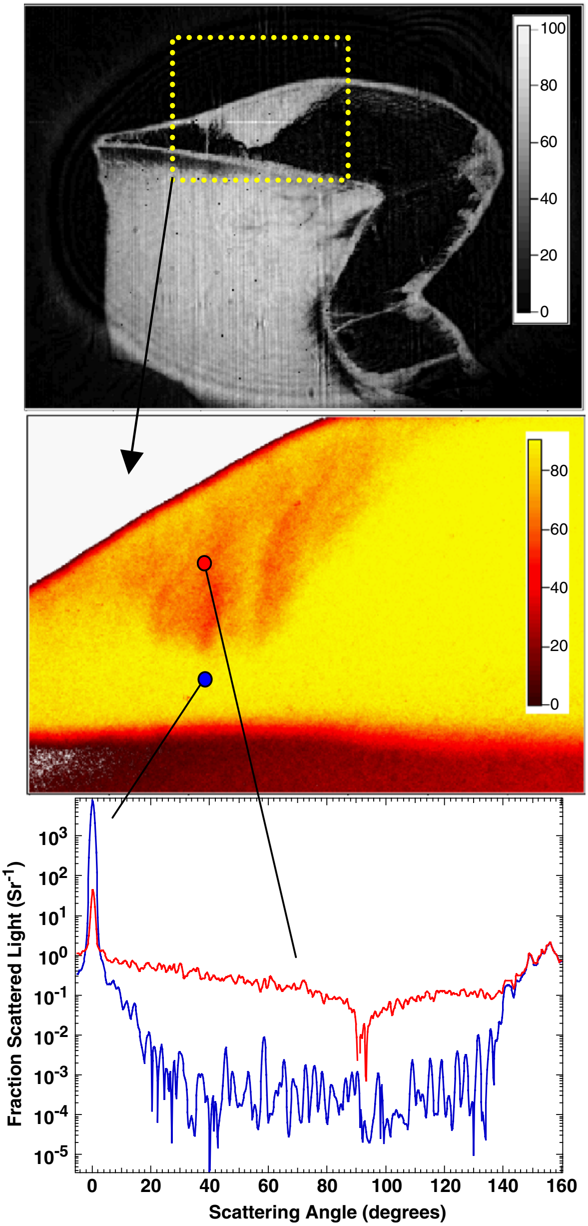

Fig. 2. (*Top*) Image of NIR (1310 nm) optical attenuation through a 200-μm thick tooth section with a natural caries lesion in the yellow box. The attenuation coefficient, μ_t, is in units of cm^{-1} and ranges from 0 to 180. (*Middle*) A high-resolution digital microradiograph of the lesion area shows the vol % mineral versus position in the lesion area. (*Bottom*) The fraction of NIR (1310 nm) light scattered versus the angle in the sound (*blue*) and carious (*red*) areas of the sample measured with the scattering goniometer.

represent more opaque regions, whereas the dark areas are more transparent. The attenuation in the lesion approaches 180 cm^{-1}, a factor 50 times higher than that of sound enamel, 2 to 3 cm^{-1}, and is of similar magnitude to that of the dentin. A high-resolution digital microradiograph of the carious region of the section is shown in the middle of Fig. 2. The volume percent (vol %) of mineral is represented by the yellow-red color table, with the areas of lower mineral content, caries lesion, and dentin in red, and the high mineral areas, namely, sound enamel, demarcated in yellow. Optical scattering measurements were taken in sound and carious regions of the same section using the scattering goniometer (see Fig. 2), as indicated by the two red and blue points in the microradiograph using a 1310-nm diode laser focused to a spot size of 100 μm. Angularly resolved scattering measurements taken at those two points are plotted in the lower part of Fig. 2. The ballistic light is reduced by two orders of magnitude, and the intensity of the light scattered at angles greater than 10 degrees is two to three orders of magnitude higher for the carious tissue over the sound enamel.

NIR optical property measurements during the longitudinal development of early artificial demineralization suggest a rapid exponential increase in optical scattering during initial lesion development followed by a more gradual increase in scattering as the lesion severity increases. This change can clearly be seen in Fig. 3, which shows goniometer measurements of angularly resolved scattering from artificially demineralized enamel over a period of 5 days of lesion progression of a 200-μm thick section of enamel. Note the rapid order of the magnitude increase in attenuation after just 1 day, followed by an increase in another order of magnitude after the next 4 days. The scattering anisotropy of demineralized enamel also seems to be highly forward directed. This observation is not entirely unexpected. Because demineralization proceeds along the core of the enamel rods, the scattering centers may be large in the micron range and highly anisotropic. Monte Carlo simulations on natural and artificial caries lesions indicate that the scattering coefficient increases by two orders of magnitude, whereas the phase function remains similar with a high-scattering anisotropy ($g = 0.96$) at 1310 nm. The optical parameters are $g = 0.96$, $f_d = 0.55$, and $\mu_s = 3\ cm^{-1}$ for sound enamel at 1310 nm.

Measurements suggest that the image contrast provided by changes in light scattering is much higher than the image contrast provided by variations in tissue density that occurs at x-ray wavelengths in dental radiography; therefore, NIR imaging methods can be expected to be more sensitive to early demineralization than x-rays.

Polarization sensitive optical coherence tomography

The authors have used an all-fiber–based OCDR system with polarization-maintaining (pm) optical fiber, high-speed piezoelectric fiber stretchers,

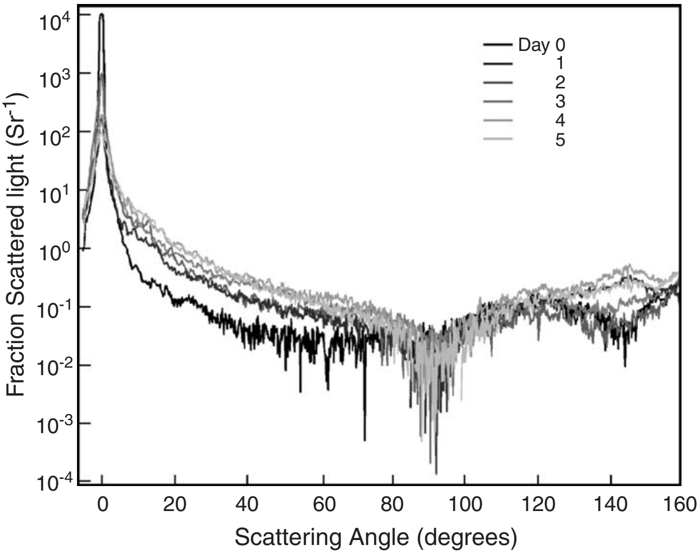

Fig. 3. Scattering distributions of 200-μm thick sections of enamel with artificial caries lesions produced by pH cycling for 0 to 5 days measured at 1310 nm. Each trace is the average of five measurements on five different samples. (*From* Huynh GD, Darling CL, Fried D. Changes in the optical properties of dental enamel at 1310-nm after demineralization. In: Lasers in dentistry X, vol. 5313. San Jose (CA): The International Society for Optical Engineering; 2004. p. 122; with permission.)

and two balanced InGaAs receivers (Optiphase, Van Nuys, California) to acquire images of caries lesions. This two-channel system was integrated with broadband high-power superluminescent diodes (SLDs) and a high-speed XY-scanning system for in vitro optical tomography. The system was based on a polarization-sensitive Michelson white light interferometer. The high-power (20 mW) polarized SLD sources operated at a center wavelength of 1310 nm. A spectral bandwidth FWHM of 50 nm was aligned using a polarization controller to deliver 20 mW into the slow axis of the pm fiber of the source arm of the interferometer. This light was split into the reference and sample arms of the Michelson interferometer by a 50/50 pm-fiber coupler. A schematic of the system is shown in Fig. 4. The system is described in more detail elsewhere [64]. An excellent text explaining the mechanics of OCT and PS-OCT has been published by Bouma and Tearney [24].

Each scan of reflectivity from within the tooth is called an a-scan. Adjacent a-scans are compiled into b-scan files. The pm fiber propagates both polarization states of the light: the parallel (||) linear polarization that is aligned with the slow axis of the pm fiber, and the perpendicular polarization (⊥) that is aligned with the fast axis of the pm fiber (Fig. 5). The light incident on the tooth is aligned with the slow axis of the fiber, that

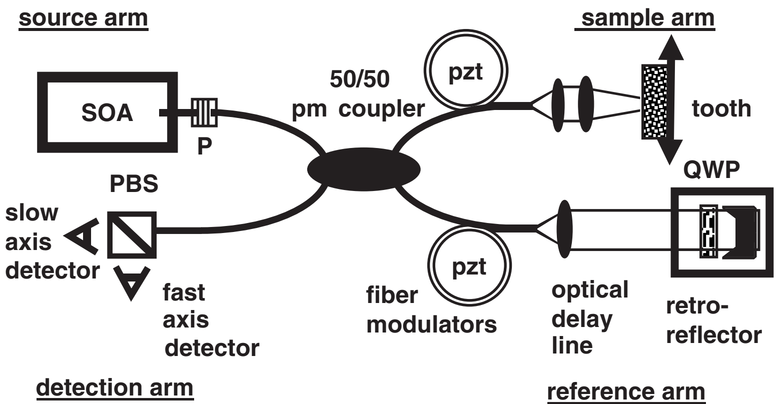

Fig. 4. PS-OCT system. Light from a semiconductor optical amplifier (SOA) or SLD is linearly polarized (P) and coupled into the slow axis of pm fiber and equally split between the sample and reference arms of a fiberoptic Michelson interferometer. The length of the reference arm can be adjusted manually using a linear stage to match the sample arm length. A modulated piezoelectric fiber stretcher (pzt) varies the length between the sample and reference arms by 6.8 mm. A polarizing beam splitter (PBS) in the detection arm splits the fast and slow axis components of the light onto two detectors.

is, ||-polarization, and any light that is directly reflected from the tooth surface remains in that state. The strong reflection from the tooth surface interferes with imaging the surface of caries lesions. This interference can be eliminated by using the perpendicular polarization, the ⊥-axis. There are two mechanisms by which intensity can arise in the perpendicular axis. The native birefringence of the tooth enamel can rotate the phase angle of the

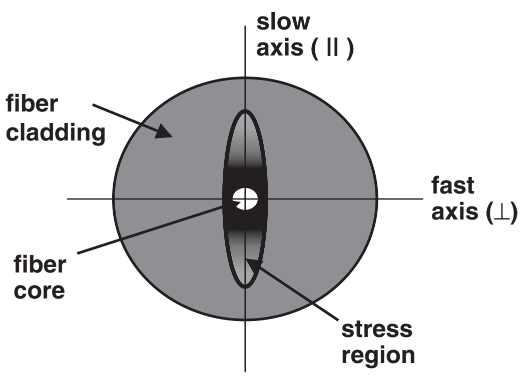

Fig. 5. Diagram of a cross-section of a pm fiber. The fiber is deliberately stressed to induce birefringence that far exceeds transient stresses induced by moving and flexing the fiber. This step preserves the polarization of the light entering the fiber. By convention, the incident light from the source is linearly polarized along the slow axis of the fiber that is also typically called the parallel axis (||). The fast axis of the fiber is the perpendicular axis (⊥).

incident light beam between the two orthogonal axes (similar to a waveplate) as the light propagates through the enamel without changing the degree of polarization. The other mechanism is depolarization from scattering in which the degree of polarization is reduced. The later mechanism is exploited to quantify the lesion severity. Complete depolarization of the incident linearly polarized light leads to an equal distribution of the intensity in both orthogonal axes. Demineralization of the enamel owing to dental decay causes an increase in the scattering coefficient by one to two orders of magnitude; therefore, demineralized enamel induces a large increase in the reflectivity along with depolarization. This increase, in turn, causes a large rise in the perpendicular polarization channel or axis.

PS-OCT images of sound, natural, and artificial demineralized enamel demonstrate that one can image about 1 to 2 mm deep in sound enamel using the current system. Highly scattering structures, such as dentin at the dentinoenamel junction (Fig. 6), and carious dentin can be detected to a depth of 2 to 3 mm beneath sound enamel; therefore, "hidden" dentinal caries can be detected. The system has an axial (depth) resolution of 20 μm that is sufficient to resolve the structure of the caries lesion, such as the surface zone that is of particular importance for determining whether the lesion is active or progressing. Longitudinal studies have demonstrated that PS-OCT can be used for monitoring erosion and demineralization. The progression of artificially produced caries lesions in the pit and fissure systems of extracted molars can be monitored nondestructively (Fig. 7), and the integrated reflectivity in the $\perp$-axis correlates well with the growth of the lesion. These factors are a major step forward in demonstrating that PS-OCT can be used to track lesion progression in vivo. Other optical methods such as QLF and conventional OCT rely on the loss of light penetration through fairly uniform lesions to estimate lesion severity, as opposed to direct measurement of the reflectivity from the lesion. That characteristic makes it difficult to apply these techniques to highly convoluted surfaces where almost all decay is found, or to natural lesions that are almost never of uniform size or severity. Moreover, using conventional OCT, one cannot differentiate the strong reflectance from the tooth surface from increased reflectivity from the lesion. Because the most important information about the lesion is near the surface, the PS-OCT system is invaluable for imaging dental caries, particularly early lesions. By exploiting depolarization in the $\perp$- axis of the PS-OCT system, one can quantify lesion severity on highly convoluted surfaces.

The PS-OCT system can also be used to image secondary caries under sealants, where the advantage of having the ability to integrate directly the PS-OCT fast axis ($\perp$-axis) images to quantify lesion severity is even more apparent [65]. The penetration depth of PS-OCT through composite is sufficient to resolve early demineralization under the sealant or restoration. The composite reflectivity, depolarization, and penetration depth are not

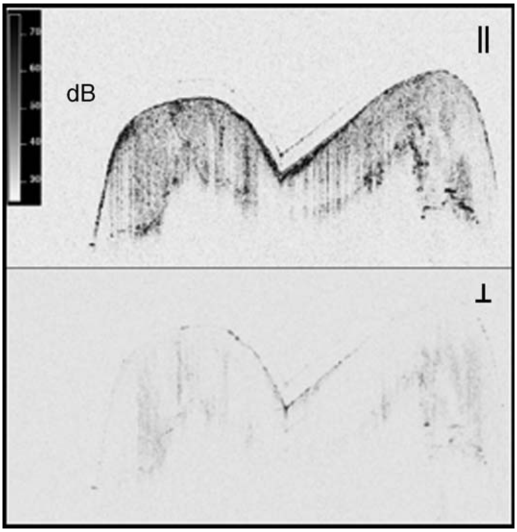

Fig. 6. ||-axis (*top*) and ⊥-axis PS-OCT scans taken using a high power 50-mw, 33-nm superluminescent (SLD) diode light-source. The intensity is shown in decibels (dB).

influenced by the composition of the filler; however, the reflectivity is markedly increased in sealants with an added optical opacifier such as titanium dioxide. Fig. 8 shows ||- and ⊥-axis PS-OCT images of the occlusal surface of a tooth subjected to 14 days of pH cycling to generate an artificial lesion approximately 100 μm in depth. Images are shown before and after placement of a sealant. This particular sealant is invisible in the perpendicular polarization state (see Fig. 8D), which facilitates direct integration of the reflectivity from the demineralized area. These images demonstrate that polarization sensitivity is necessary for differentiating demineralized enamel under composite sealants and restorations.

It is not sufficient to simply detect a carious lesion or areas of demineralization. It is also necessary to assess the state of the carious lesion and to determine whether it is active and progressing, or arrested and remineralizing. One can take two approaches for determining the state of activity of carious lesions. The first approach is based on monitoring the lesion progression over time to determine whether it changes (see Fig. 7). The second approach is to examine the structure of the lesion to determine whether there are any definitive features, such as a weakly scattering surface zone, that are indicative of remineralization. Elkstrand has recently described the pathoanatomic changes in enamel during caries initiation, progression, and arrestment [66]. The surfaces of arrested lesions are typically hard and shiny with less light scattering, in contrast to the soft and chalky surface of active lesions. One can postulate that if PS-OCT can resolve changes in lesion structure and demineralization, for example, the presence of a surface zone of reduced light scattering, this method may have

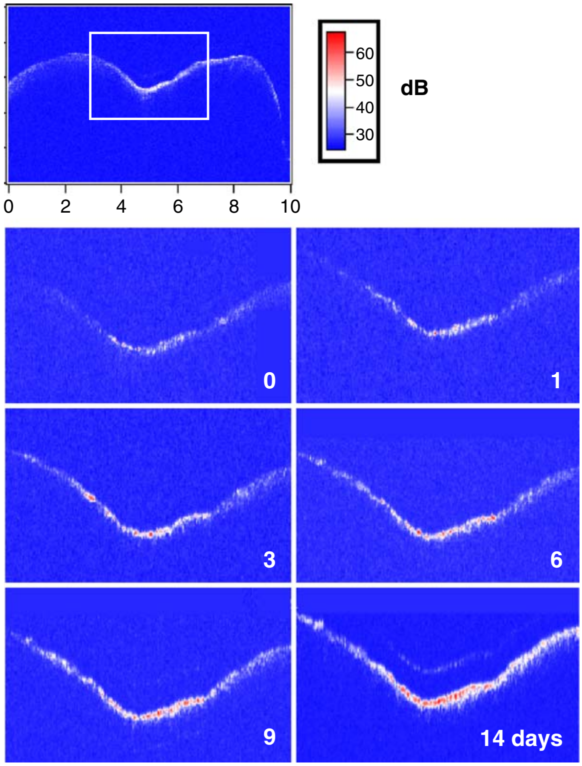

Fig. 7. Serial PS-OCT scans of a molar after pH cycling. The upper left image is the ||-axis scan at day 0. Red areas are of higher reflectivity; blue areas are the noise floor. The lower six ⊥-axis images represent the reflectivity after 0 to 14 days of demineralization.

potential as a quantitative diagnostic tool to determine the activity of the lesion. The integrated reflectivity of the ⊥-axis PS-OCT images of natural lesions correlates well with the integrated mineral loss and can be used to measure lesion severity directly. Fig. 9 shows the ⊥-axis PS-OCT and digital microradiography images of a pigmented lesion. Five PS-OCT line profiles were taken at different positions in the lesion, and each was integrated to yield a total integrated reflectivity for that area of the lesion to a depth of 500 μm. The integrated reflectivity correlated well with the matching mineral density profiles taken from the digital microradiographic images that were integrated to yield the lesion mineral loss or ΔZ value. PS-OCT images also accurately represent the highly convoluted internal structure of caries lesions.

Using PS-OCT, depolarization of the incident light by the caries lesion can be exploited to facilitate direct integration of the lesion reflectivity to quantify the lesion severity, regardless of the tooth topography. The difficult task of having to deconvolve the strong surface reflection from the lesion

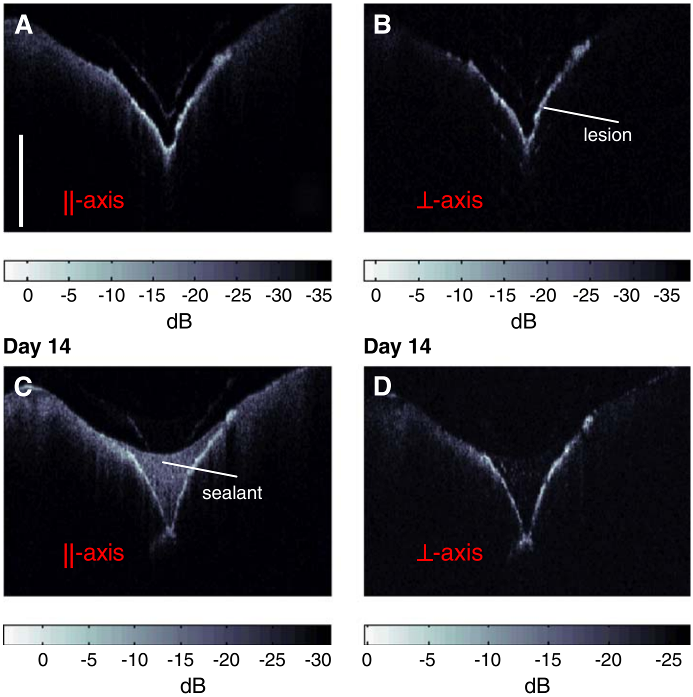

Fig. 8. PS-OCT images of artificial lesions after 14 days of pH cycling without (*A, B*) and with (*C, D*) Aeliteflo sealants (no opacifier). In the parallel axis (*A, C*), surface reflections can mask the subsurface demineralization, and the sealant is clearly visible. In the perpendicular axis, only depolarization from the lesion is visible, and the sealant that does not depolarize the light is not visible. The vertical white bar is 1 mm. (*From* Jones RS, Staninec M, Fried D. Imaging artificial caries under composite sealants and restorations. J Biomed Opt 2004;9(6):1303; with permission.)

surface can be circumvented. This factor is of particular importance when looking at the surface structure of caries lesions for the presence of a surface zone indicative of remineralization. Moreover, recent studies suggest that polarization sensitivity can be used to differentiate between composites and tooth structure and can even differentiate different composites [65]. These studies clearly demonstrate that a clinical OCT system will require polarization sensitivity to be able to quantify lesion severity in vivo.

Near-infrared imaging and transillumination of caries lesions

Enamel is virtually transparent in the NIR, with optical attenuation one to two orders of magnitude less than in the visible range. Transmission measurements through demineralized tissue sections at 1310 nm show that the demineralized tissue attenuates the laser beam by a factor 20 to 50 times greater than sound enamel [67,68]; therefore, the NIR spectrum is ideal for

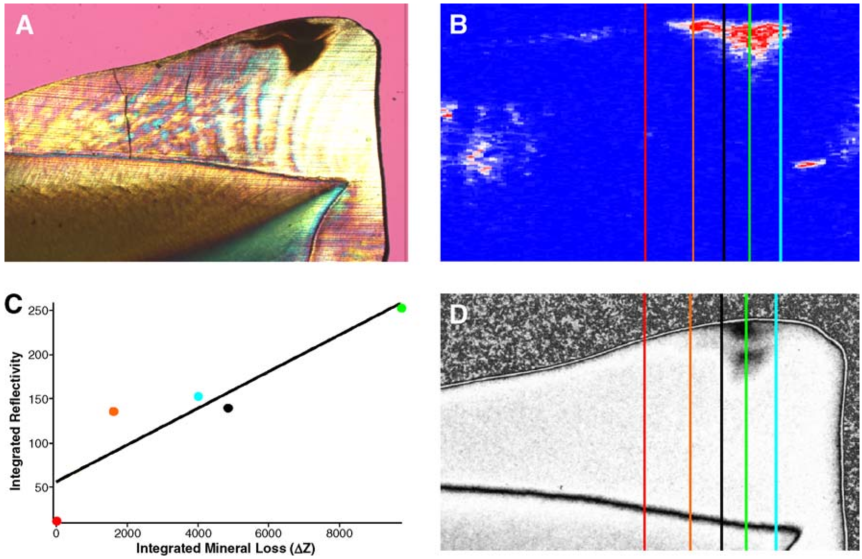

Fig. 9. (*A*) Reflected light image of lesion. (*B*) ⊥-axis PS-OCT scan. It is necessary to compare the ||- and ⊥-scans to see the position of the tooth surface because the surface zone is not visible in the ⊥-axis scan. (*C*) Plot of the integrated reflectivity and the integrated mineral loss determined with digital microradiography taken from (*D*) for the five line profiles indicated by the colored lines on each image. There was a strong correlation (r = 0.92, Pearson). Red is high reflectivity, blue is low reflectivity (*B*), and black is reduced mineral density (*D*).

imaging caries lesions. The authors have employed two NIR systems to image caries. The first system uses an InGaAs focal plane array that can operate from 1000 to 1600 nm. The second system employs a low-cost CCD camera that can be used for imaging at 830 nm. Images were acquired of simulated and natural caries lesions on extracted human teeth. Two setups were employed in these studies (Fig. 10), one optimized for imaging interproximal lesions through transillumination of teeth, and another that enabled the acquisition of fairly uniform high-contrast images of occlusal lesions. Various light sources were investigated for NIR imaging, including fabry-perot NIR diode lasers, tungsten-halogen lamps, and broadband SLDs. The SLDs provided a high-intensity uniform illumination source from an optical fiber, and the high bandwidth avoided the production of laser speckle for better images.

High contrast can be achieved at 1310 nm between simulated and natural caries lesions and sound tissues [69]. Simulated lesions were used to determine the image contrast at various wavelengths as a function of enamel thickness. The lesions were produced by drilling small 1-mm diameter cavities on the mesial or distal aspect of tooth sections of varying thickness or whole teeth. An anterior whole tooth is shown in Fig. 11 with a simulated interproximal lesion. A hole was drilled in the side of the tooth as shown in

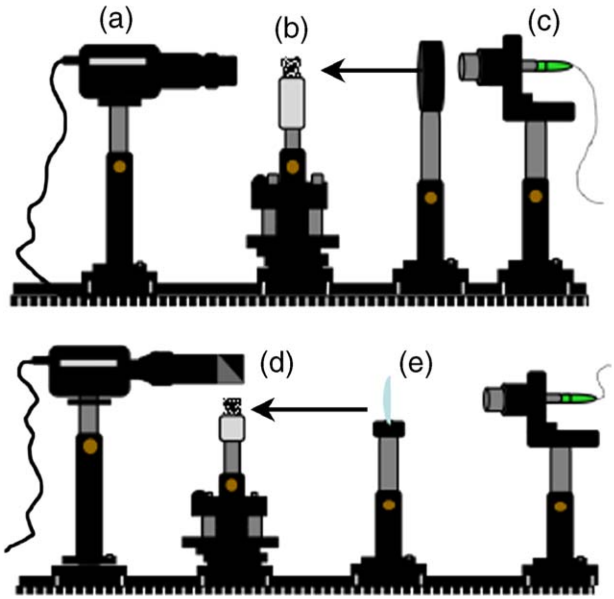

Fig. 10. Setup for NIR (*top*) transillumination of interproximal lesions and (*bottom*) occlusal lesions. InGaAs FPA with lens (*a*) or right-angle prism to view the occlusal surface (*d*) of the tooth (*b*). Illumination was provided by an SLD with collimator/polarizer (*c*), or a 20-mm collimator and cylindrical lens (*e*).

Fig. 11D, and the cavity was filled with a hydroxyapatite paste with the same refractive index as enamel and of reduced density. The grain boundaries of the powder serve as scattering sites, replicating the scattering sites produced in caries lesions. A bite-wing radiograph (see Fig. 11B) is shown for comparison. The lesion is clearly more visible with NIR light. Better image contrast is achievable owing to light scattering at NIR wavelengths than that provided by changes in tissue density at x-ray wavelengths. The lesion cannot be seen at all in the visible range with a conventional CCD camera (see Fig. 11C). Note that a dark stain on the upper right surface of the tooth also looks like a caries lesion in the visible range. This confounding stain does not appear on the NIR image. In the NIR images, it is easier to differentiate stains from demineralization. Images taken through plano-parallel tooth sections, up to 6.75 mm in thickness, show that the simulated lesions can be resolved through the maximum possible thickness of enamel.

The imaging system operating near 830 nm using a low-cost silicon CCD optimized for the NIR is capable of significantly higher performance than a visible system but does not provide as high a contrast as that attainable at 1310 nm [70]. Images of anterior teeth with natural interproximal lesions demonstrate that the system can be used on larger premolars and molars

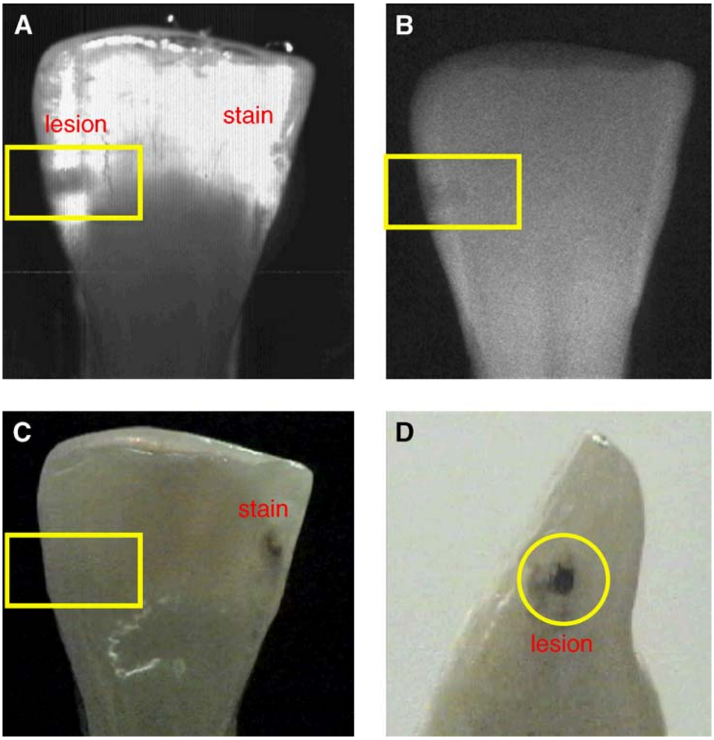

Fig. 11. Comparison of (*A*) NIR image, (*B*) x-ray (D-speed film), (*C*) visible image of an anterior tooth with a simulated interproximal lesion, and (*D*) side view of the tooth showing the lesion surface and position. The stain on the buccal surface is not visible on the NIR image.

(Fig. 12). Nevertheless, posterior teeth pose a considerable challenge owing to their large size, reduced enamel, and high surface curvature, and methods need to be developed to reduce the confounding influence of refraction and internal reflection on highly curved surfaces to enhance image contrast.

Occlusal images were acquired by illuminating the tooth with a "sheet of 1310-nm light" just above the gingiva from one side using a cylindrical lens. The camera or endoscope was positioned directly above the occlusal surface as shown in Fig. 10 so that diffuse light propagated up through the enamel of the crown from the underlying dentin [71]. These initial images show that NIR imaging can be used for discriminating demineralization, staining, and pigmentation, and developmental defects such as fluorosis. Organic stains are not visible in the NIR at 1310 nm. In Fig. 13A to C, an NIR image, a visible reflected light image, and an x-ray (D-speed film) of a molar containing an occlusal lesion with extensive staining are shown. The tooth is covered with white spots owing to early demineralization or fluorosis (developmental defect). The NIR image (see Fig. 13A) shows a large optical opacity (dark area) owing to a broad area of demineralization. This lesion

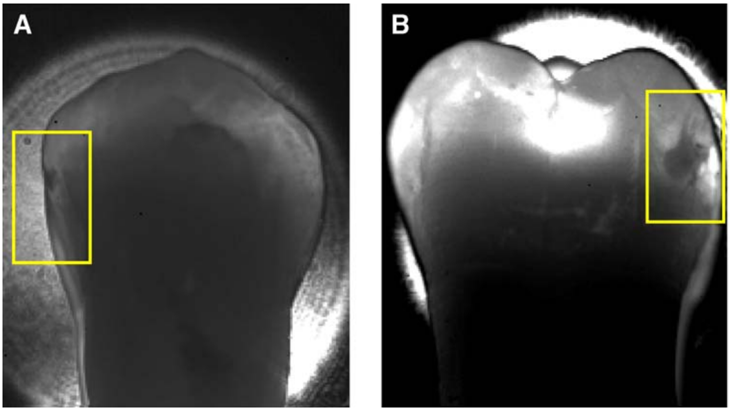

Fig. 12. NIR images of natural interproximal lesions on two posterior teeth, with lesions in yellow boxes. (*A*) Shallow lesion. (*B*) Deep cavitated lesion. The empty cavitated area between the lesion and the tooth surface does not show up in the NIR image, whereas on the x-ray, only the cavitated area is visible and the demineralized area is not. If the area of decay does not connect with the surface, there is a region of cavitation in between.

extends into the dentin and is barely visible on the radiograph in Fig. 13C. The white spots most likely caused by fluorosis still appear white in the NIR transillumination images, in contrast to demineralized areas that appear darker owing to attenuation of the light coming up from the tooth center. Apparently, neither staining nor developmental defects such as fluorosis interfere significantly with NIR imaging of demineralization. Although dental calculus is highly opaque in NIR images, it stands out from the surface, allowing differentiation from demineralization.

Based on these initial images, one can hypothesize that the NIR system can be used to differentiate among staining, developmental defects, and demineralization and will improve the ability of clinicians to localize areas of demineralization. The NIR image of a second molar in Fig.13D shows highly localized shallow decay along some of the fissures. This image demonstrates that fissures appear optically opaque owing to the localized demineralization and not because of the fissure topography. This characteristic is an important distinction from the appearance on imaging reflected light, in which fissures appear darker simply due to lower reflectivity. Another molar with localized occlusal decay is shown in Fig. 13E to F. The image in Fig. 13E was taken with the camera lens and the image in Fig. 13F with an endoscope to demonstrate the ease in acquiring in vivo NIR occlusal images of posterior teeth. NIR images also have great potential for examining defects in tooth structure, and cracks in enamel can be clearly resolved with this method.

Optical diagnostic tools operating in the NIR have considerable potential for imaging early caries lesions owing to the high transparency of enamel. One can envisage using NIR transillumination imaging to screen for dental

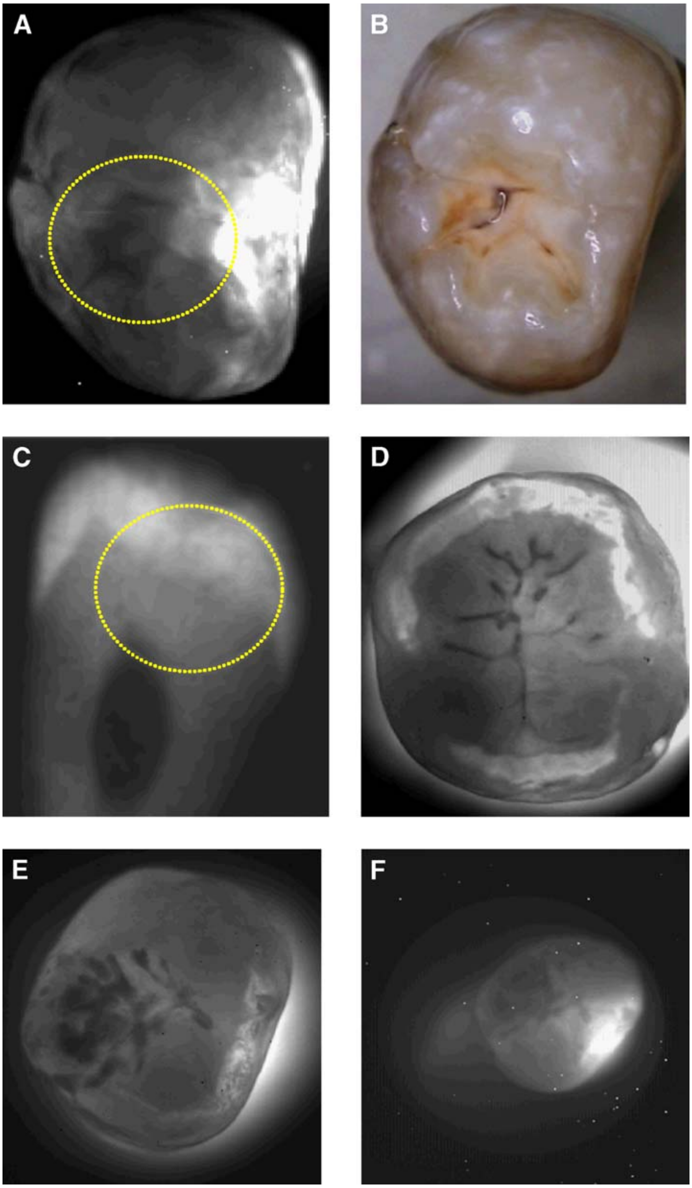

Fig. 13. NIR occlusal images of molars with carious lesions. (*A*) NIR and (*B*) visible reflected light images of a molar with a large lesion (yellow circle) that penetrates into the dentin and that can barely be resolved on (*C*) an x-ray (D-speed) film. Another molar (*D*) has shallow lesions localized to a few fissures, whereas a third molar (*E*) has decay on one quadrant of the tooth, which can also be easily resolved with an endoscope (*F*).

caries in conjunction with PS-OCT to probe suspect occlusal lesions to ascertain lesion depth and severity. PS-OCT is very promising for tracking lesion progression over time and for quantifying lesion severity, and can potentially be used for in vivo testing of anticaries agents in clinical trials on a much shorter time scale than previously used. The next step is to build clinical prototypes, collect in vivo images, and assess the performance of these NIR imaging tools in the clinical setting.

Acknowledgments

The authors would like to acknowledge the contributions of John Xie, Gigi Huynh, and Charles Q. Le.

References

[1] National Institutes of Health. Diagnosis and management of dental caries throughout life: NIH consensus statement. Washington (DC): National Institutes of Health; 2001.
[2] Lussi A. Validity of diagnostic and treatment decisions of fissure caries. Caries Res 1991;25: 296–303.
[3] Featherstone JDB, Young D. The need for new caries detection methods. In: Lasers in Dentistry V, vol. 3593. San Jose (CA): The International Society for Optical Engineering; 1999. p. 134–40.
[4] Hume WR. Need for change in dental caries diagnosis. In: Stookey GK, editor. Early detection of dental caries. Indianapolis (IN): Indiana University; 1996. p. 1–10.
[5] Featherstone JDB. Clinical implications: new strategies for caries prevention. In: Stookey GK, editor. Early detection of dental caries. Indianapolis (IN): Indiana University; 1996. p. 287–96.
[6] ten Cate JM, van Amerongen JP. Caries diagnosis: conventional methods. In: Stookey GK, editor. Early detection of dental caries. Indianapolis (IN): Indiana University; 1996. p. 27–37.
[7] Featherstone JDB. Prevention and reversal of dental caries: role of low level fluoride. Community Dent Oral Epidemiol 1999;27:31–40.
[8] Pine CM. Fiber-optic transillumination (FOTI) in caries diagnosis. In: Stookey GK, editor. Early detection of dental caries. Indianapolis (IN): Indiana University; 1996. p. 51–66.
[9] Peltola J, Wolf J. Fiber optics transillumination in caries diagnosis. Proc Finn Dent Soc 1981;77:240–4.
[10] Barenie J, Leske G, Ripa LW. The use of fiber optic transillumination for the detection of proximal caries. Oral Surg 1973;36:891–7.
[11] Holt RD, Azeevedo MR. Fiber optic transillumination and radiographs in diagnosis of approximal caries in primary teeth. Community Dent Health 1989;6:239–47.
[12] Mitropoulis CM. The use of fiber optic transillumination in the diagnosis of posterior approximal caries in clinical trials. Caries Res 1985;19:379–84.
[13] Schneiderman A, Elbaum M, Schultz T, et al. Assessment of dental caries with digital imaging fiber-optic transillumination (DIFOTI): in vitro study. Caries Res 1997;31:103–10.
[14] Alfano RR, Lam W, Zarrabi HJ, et al. Human teeth with and without caries studied by laser scattering, fluorescence and absorption spectroscopy. IEEE J Quant Electr 1984;20:1512–5.
[15] Bjelkhagen H, Sundstrom F. A clinically applicable laser luminescence for the early detection of dental caries. IEEE J Quant Electr 1981;17:266–8.

[16] Hafstrom-Bjorkman U, Sundstrom F, de Josselin de Jong E, et al. Comparison of laser fluorescence and longitudinal microradiography for quantitative assessment of in vitro enamel caries. Caries Res 1992;26:241–7.
[17] Ando M, Gonzalez-Cabezas C, Isaacs RL, et al. Evaluation of several techniques for the detection of secondary caries adjacent to amalgam restorations. Caries Res 2004;38:350–6.
[18] Fontana M, Li Y, Dunipace AJ, et al. Measurement of enamel demineralization using microradiography and confocal microscopy. Caries Res 1996;30:317–25.
[19] de Josselin de Jong E, Sundstrom F, Westerling H, et al. A new method for in vivo quantification of changes in initial enamel caries with laser fluorescence. Caries Res 1995;29: 2–7.
[20] Koenig K, Schneckenburger H, Hemmer J, et al. In-vivo fluorescence detection and imaging of porphyrin-producing bacteria in the human skin and in the oral cavity for diagnosis of acne vulgaris, caries, and squamous cell carcinoma. In: Advances in laser and light spectroscopy to diagnose cancer and other diseases, vol. 2135. San Jose (CA): The International Society for Optical Engineering; 1994. p. 129–38.
[21] Shi XQ, Welander U, Angmar-Mansson B. Occlusal caries detection with Kavo DIAGNOdent and radiography: an in vitro comparison. Caries Res 2000;34:151–8.
[22] Hibst R, Paulus R. New approach on fluorescence spectroscopy for caries detection. In: Lasers in Dentistry V, vol. 3593. San Jose (CA): The International Society for Optical Engineering; 1999. p. 141–8.
[23] Lussi A, Imwinkelreid S, Pitts NB, et al. Performance and reproducibility of a laser fluorescence system for detection of occlusal caries in vitro. Caries Res 1999;33:261–6.
[24] Bouma BE, Tearney GJ, editors. Handbook of optical coherence tomography. New York: Marcel Dekker; 2002.
[25] Derickson D. Fiber optic test and measurement. Upper Saddle River (NJ): Prentice Hall; 1998.
[26] Youngquist RC, Carr S, Davies DEN. Optical coherence-domain reflectometry. Appl Opt 1987;12:158–60.
[27] Huang D, Swanson EA, Lin CP, et al. Optical coherence tomography. Science 1991;254: 1178–81.
[28] Colston B, Everett M, Da Silva L, et al. Imaging of hard and soft tissue structure in the oral cavity by optical coherence tomography. Appl Opt 1998;37(19):3582–5.
[29] Colston BW, Everett MJ, Da Silva LB, et al. Optical coherence tomography for diagnosis of periodontal diseases. In: Coherence domain optical methods in biomedical science and clinical applications II, vol. 3251. San Jose (CA): The International Society for Optical Engineering; 1998. p. 52–8.
[30] Colston BW, Sathyam US, DaSilva LB, et al. Dental OCT. Opt Express 1998;3(3):230–8.
[31] Baumgartner A, Hitzenberger CK, Dicht S, et al. Optical coherence tomography for dental structures. In: Lasers in Dentistry IV, vol. 3248. San Jose (CA): The International Society for Optical Engineering; 1998. p. 130–6.
[32] Dicht S, Baumgartner A, Hitzenberger CK, et al. Polarization-sensitive optical coherence tomography of dental structures. In: Lasers in Dentistry V, vol. 3593. San Jose (CA): The International Society for Optical Engineering; 1999. p. 169–76.
[33] Baumgartner A, Dicht S, Hitzenberger CK, et al. Polarization-sensitive optical coherence tomography of dental structures. Caries Res 2000;34:59–69.
[34] Feldchtein FI, Gelikonov GV, Gelikonov VM, et al. In vivo OCT imaging of hard and soft tissue of the oral cavity. Opt Express 1998;3(3):239–51.
[35] Wang XJ, Zhang JY, Milner TE, et al. Characterization of dentin and enamel by use of optical coherence tomography. Appl Opt 1999;38(10):586–90.
[36] Everett MJ, Colston BW, Sathyam US, et al. Non-invasive diagnosis of early caries with polarization sensitive optical coherence tomography (PS-OCT). In: Lasers in Dentistry V, vol. 3593. San Jose (CA): The International Society for Optical Engineering; 1999. p. 177–83.

[37] Otis LL, Al-Sadhan RI, Meiers J, et al. Identification of occlusal sealants using optical coherence tomography. J Clin Dent 2003;14(1):7–10.
[38] Amaechi BT, Higham SM, Podoleanu AG, et al. Use of optical coherence tomography for assessment of dental caries. J Oral Rehab 2001;28(12):1092–3.
[39] Amaechi BT, Podoleanu A, Higham SM, et al. Correlation of quantitative light-induced fluorescence and optical coherence tomography applied for detection and quantification of early dental caries. J Biomed Optics 2003;8(4):642–7.
[40] Zijp JR, ten Bosch JJ. Angular dependence of HeNe laser light scattering by bovine and human dentine. Archs Oral Biol 1991;36:283–9.
[41] Zijp JR, ten Bosch JJ. Theoretical model for the scattering of light by dentin and comparison with measurements. Appl Opt 1993;32:411–5.
[42] Fried D, Featherstone JDB, Glena RE, et al. The nature of light scattering in dental enamel and dentin at visible and near-IR wavelengths. Appl Opt 1995;34(7):1278–85.
[43] Zijp JR, ten Bosch JJ, Groenhuis RA. HeNe laser light scattering by human dental enamel. J Dent Res 1995;74:1891–8.
[44] Schmidt WJ, Keil A. Polarizing microscopy of dental tissues. Tarrytown (NY): Pergamon Press; 1971.
[45] Theuns HM, Shellis RP, Groeneveld A, et al. Relationships between birefringence and mineral content in artificial caries lesions in enamel. Caries Res 1993;27:9–14.
[46] Cheong W, Prahl SA, Welch AJ. A review of the optical properties of biological tissues. IEEE J Quant Electr 1990;26:2166–85.
[47] Wilson BC, Patterson MS, Flock ST. Indirect versus direct techniques for the measurement of the optical properties of tissues. Photochem Photobiol 1987;46(5):601–8.
[48] Izatt JA, Hee MR, Huang D, et al. Optical coherence tomography for medical applications. In: Muller G, Chance B, Alfano R, et al, editors. Medical optical tomography: functional imaging and monitoring, vol. IS11. Bellingham (WA): The International Society for Optical Engineering; 1993. p. 450–72.
[49] Tuchin V. Tissue optics: light scattering methods and instruments for medical diagnostics, vol. TT38. Bellingham (WA): The International Society for Optical Engineering; 2000.
[50] Spitzer D, ten Bosch JJ. The absorption and scattering of light in bovine and human dental enamel. Calcif Tissue Res 1975;17:129–37.
[51] ten Bosch JJ, Zijp JR. Optical properties of dentin. In: Thylstrup A, editor. Dentine and dentine research in the oral cavity. Oxford (UK): IRL Press; 1987. p. 59–65.
[52] Jones RS, Fried D. Attenuation of 1310-nm and 1550-nm laser light through sound dental enamel. In: Lasers in Dentistry VIII, vol. 4610. San Jose (CA): The International Society for Optical Engineering; 2002. p. 187–90.
[53] Hale GM, Querry MR. Optical constants of water in the 200-nm to 200-μm wavelength region. Appl Opt 1973;12:555–63.
[54] Monte Carlo modeling of light transport in multi-layer tissues in standard C [computer program]. Version 1.0. Houston (TX): University of Texas, M.D. Anderson Cancer Center; 1992.
[55] Wilson BC, Adam G. A Monte Carlo model for the absorption and flux distribution of light in tissue. Med Phys 1989;10:824–30.
[56] Van der Zee P. Methods for measuring the optical properties of tissue in the visible and near-IR wavelength range. In: Medical optical tomography: functional imaging and monitoring, vol. IS11. Bellingham (WA): The International Society for Optical Engineering; 1993. p. 450–72.
[57] Brinkman J, ten Bosch JJ, Borsboom PCF. Optical quantification of natural caries in smooth surfaces of extracted teeth. Caries Res 1988;22:257–62.
[58] ten Bosch JJ, van der Mei HC, Borsboom PCF. Optical monitor of in vitro caries. Caries Res 1984;18:540–7.
[59] Angmar-Mansson B, ten Bosch JJ. Optical methods for the detection and quantification of caries. Adv Dent Res 1987;1(1):14–20.

[60] ten Bosch JJ, Coops JC. Tooth color and reflectance as related to light scattering and enamel hardness. J Dent Res 1995;74:374–80.
[61] Ko CC, Tantbirojn D, Wang T, et al. Optical scattering power for characterization of mineral loss. J Dent Res 2000;79(8):1584–9.
[62] Wefel JS, Clarkson BH, Heilman JR. Natural root caries: a histologic and microradiographic evaluation. J Oral Pathol 1985;14:615–23.
[63] Vaarkamp J, Bosch JJ, Verdonschot EH. Light propagation through teeth containing simulated caries lesions. Phys Med Biol 1995;40:1375–87.
[64] Fried D, Xie J, Shafi S, et al. Early detection of dental caries and lesion progression with polarization sensitive optical coherence tomography. J Biomed Opt 2002;7(4):618–27.
[65] Jones RS, Staninec M, Fried D. Imaging artificial caries under composite sealants and restorations. J Biomed Opt 2004;9(6):1297–304.
[66] Ismail AI. Visual and visuo-tactile detection of dental caries. J Dent Res 2004;83(Special Issue C):C56–66.
[67] Huynh GD, Darling CL, Fried D. Changes in the optical properties of dental enamel at 1310-nm after demineralization. In: Lasers in Dentistry X, vol. 5313. San Jose (CA): The International Society for Optical Engineering; 2004. p. 118–24.
[68] Darling CL, Fried D. Optical properties of natural caries lesions in dental enamel at 1310-nm. In: Lasers in Dentistry XI, vol. 5687. San Jose (CA): The International Society for Optical Engineering; 2005. p. 102–10.
[69] Jones RS, Huynh GD, Jones GC, et al. Near-IR transillumination at 1310-nm for the imaging of early dental caries. Opt Express 2003;11(18):2259–65.
[70] Jones G, Jones RS, Fried D. Transillumination of interproximal caries lesions with 830-nm light. In: Lasers in Dentistry X, vol. 5313. San Jose (CA): The International Society for Optical Engineering; 2005. p. 34–41.
[71] Bühler CM, Ngaotheppitak P, Fried D. Imaging of occlusal dental caries (decay) with near-IR light at 1310-nm. In: Lasers in Dentistry XI, vol. 5687. San Jose (CA): The International Society for Optical Engineering; 2005. p. 25–33.